Simulation and analysis of water transport and evaporation under non-isothermal field conditions

Josep Mª Gastó and Jordi Grifoll

Departament d'Enginyeria Química

Escola Tècnica Superior d´Enginyeria Química

Universitat Rovira i Virgili

Tarragona

(*E-mail*: jgasto@etseq.urv.es)

Abstract

The characteristic daily oscillation cycle usually observed for the moisture content in the surface zone of a field soil has been examined via a modeling approach. A complete water and heat transport model has been formulated and implemented in a simulation code. No empirical enhancing factors have been used to describe the water vapor diffusion process. The model has been validated against field observation results corresponding to two different experimental works that constitute a reference in the literature. Simulation results obtained for a bare soil evaporation episode have shown that daily variations observed for the moisture content are governed by slightly differences between the evaporative and the water flux near surface. Both the liquid and the vapor flux are of similar magnitude and contribute to a different extent to the water transport process. A detailed analysis of the thin zone where evaporation takes place distinguishes two different zones near the soil surface: an upper dry zone where the

diffusive and dispersive transport mechanisms dominate the water transport, and a lower wet zone where the water transport is mainly achieved by convective liquid flux.

1.- Introduction

The effects of non-isothermal conditions on water transport in the unsaturated soil zone near surface have been observed by numerous authors during the last century [*Philip and de Vries*, 1957; *Cary*, 1966; *Hank et al.*, 1967, *Rose*, 1968 a,b; *Jackson et al.*, 1974; *Wescot and Wierenga*, 1974; *Milly*, 1982, 1984, 1996; *Cahill and Parlange*, 1998, *Parlange et al.*, 1998]. Many of these studies have demonstrated that the presence of temperature gradients in unsaturated soils may induce water fluxes in gas and liquid phase that can significantly contribute to the water and energy transport processes.

One of the first field-scale works that focused on the water and energy transport in the unsaturated soil correspond to Rose [*1968* a,b]. Using experimental results obtained under natural field conditions, Rose concluded that the measured water vapor fluxes were of comparable magnitude to the liquid water fluxes. Rose also observed that the direction of the vapor flux oscillated in response to the diurnal temperature gradient and, moreover, he found that the amount of water transported as vapor was on the same order of magnitude as the daily variations of the Volumetric Moisture Content (VMC) measured near surface. In a similar experimental work, Jackson studied the effects of dynamics soil water content conditions on the evaporative flux, [*Jackson*, 1973; *Jackson et al.*, 1974]. Similar to the results obtained by Rose [*1968* a,b], Jackson observed that the VMC and the soil temperature described a diurnal variation cycle characterized by night increases and day decreases. The water vapor fluxes found in Jackson's

experiment were on the same order of magnitude as the values obtained by Rose. In a later work Monji et al. [*1990*] focused on the relation between the dynamic VMC changes observed near surface and the evaporative flux. Monji observed that the VMC increased in the soil even when evaporation flux was going on. Although the author attributed this moisture increase to the water movement generated by the presence of temperature gradients in soils, he concluded that no reliable relations concerning water vapor transport were available at that moment.

The growing computational capacity of the actual computers have enhanced the use of more sophisticated and accurate simulation models for the water and energy transport in unsaturated soils. These simulation models have been useful to describe with detailed the thin zone where evaporation takes place. The work of Boulet et al. [*1997*] for example, distinguished near surface an upper dry zone where vapor flux was the most important transfer term and a lower zone where liquid flux dominated the water movement. In the case of Yamanaka et al. [*1998*] field observations and numerical experiments were carried out for different experimental conditions. The results obtained indicated that the depth where evaporation takes place changes depending on the hydraulic properties of the soil. Finally the work of Saravanapavan and Salvucci, [*2000*] explored the relative roles of vapor and liquid fluxes in rate-limiting the transfer of water from the inner soil to the atmosphere. In that work, the authors demonstrated the rate limiting role of the liquid flow. Although all these works have increased our knowledge about the water dynamics near surface, the correct description and understanding of the evaporation process and the coupled water and energy transport that take place in the unsaturated zone remains a significant challenge in hydrology, [*Saravanapavan and Salvucci*, 2000].

Possibly one of the main drawback is the absence of an adequate theory to describe vapor movement in soils near the land surface [*Cahill and Parlange*, 2000]. Usually the theoretical framework used to describe the liquid and gas fluxes under non isothermal conditions has been based on the classical Philip and de Vries formulation (henceforth PdV) [*Philip and de Vries*, 1957]. Although in many cases the application of the PdV theory to field and laboratory studies has allowed a positive comparison between experimental and simulated values, [*Milly*, 1984; *Scanlon and Milly*, 1994], in other cases and according to the results of Cahill and Parlange [*1998*], the use of the PdV framework not only had underestimates the magnitude of the vapor flux measured but it also has failed in predicting the sign of the vapor flux in soils near the land surface. Recently these authors proposed a new theoretical development for the water vapor flux based on the convective enhanced transport driven by the diurnal heating and cooling of the soil surface, [*Parlange et al.*, 1998].

The aim of the present study is to explore via a deterministic model the role and evolution of the different transport mechanisms involved in the soil drying process of a bare soil under natural atmospheric conditions. Simulation results obtained from a reliable numerical models for the coupled heat and water movement will help in understanding the mechanisms that govern the water dynamic near surface. In the model the water and heat fluxes will be described using the classical formulation adapted to the porous media without using any enhancement or tuning factor for the diffusive vapor flow. The model will be validated through simulation of two well known experiments that constitute a reference in the hydrologic field.

2.- Basic equations and solution scheme

The simulation model for the coupled heat and water transport in the unsaturated soil includes three different mass balance equations (one for the liquid water, one for the vapor water, and finally one for the gaseous phase as a whole) as well as an energy balance. The liquid water movement is modeled by means of Richards´ equation subject to dynamic surface boundary conditions. The water vapor movement is modeled considering the dependence of the vapor pressure with temperature and the decrease of vapor pressure with capillary pressure of the liquid water. In the model no empirical enhancing factors for the water vapor diffusion process have been used. The movement of the gaseous phase as a whole is due mainly to liquid water displacement and change of gas density with temperature. The energy balance equation considers conductive, convective and dispersive heat fluxes inside the porous matrix.

The top boundary condition for the water considers evaporation controlled by capillary head at surface and rain infiltration. The top boundary condition for the energy equation is expressed through an energy balance that takes into account downward and upwards radiative fluxes, convective heat flow to the atmosphere, sensible heat flux and the heat flux generated by other transport mechanisms that goes deep into the soil. The mass and energy balance equations are coupled and therefore must be solved together.

2.1 Water transport under non-isothermal conditions

The soil water movement can be described through the mass conservation equation applied to every phase involved in the transport process [*Bear and Bachmat*, 1991]. In liquid phase the mass balance for the water is:

$$\frac{\partial \theta_l \rho_l}{\partial t} = -\nabla \cdot \rho_l q_{liq} - f_{LG} \tag{1}$$

where ρ_l (kg/m^3) is the liquid water density, θ_l (m^3/m^3) is the volumetric liquid water content, q_{liq} (m/s) is the liquid phase flow and f_{LG} (kg/m^{3}s) refers to the water flow per unit volume that goes from the liquid to the gas phase. The liquid phase flow under non isothermal conditions is proportional to pressure gradient and can be expressed by means of Darcy's law [*Bear and Bachmat*, 1991]

$$q_{liq} = -\left[\frac{k_i \cdot k_r}{\mu_l} \cdot \left(\nabla P_l - \rho_l g \nabla z\right)\right] \tag{2}$$

where k_i is the intrinsic permeability, (m^2), k_r is the relative permeability, μ_l (kg/m s) is water viscosity, g (m/s^2) is the gravitational term and finally P_l (Pa) is the manometric water pressure. In this equations μ_l and ρ_l are considered to be temperature dependent and P_l depends on θ_l and temperature.

The temperature effect on P_l can be expressed through the relation [*Milly*, 1982]

$$P_l(T) = \frac{P_l\left(T^\circ\right)}{\sigma\left(T^\circ\right)}\sigma(T) \tag{3}$$

where T^o is a reference temperature and σ is the surface tension (N/m). Temperature dependence of σ has been obtained from a semi-empirical correlation based on data from *Grant and Salehzadeh* [1996].

The mass balance equation for vapor water is expressed through [*Bear and Bachmat*, 1991]:

$$\frac{\partial \theta_g \rho_v}{\partial t} = -\nabla \cdot \left(\rho_v q_{gas} + \theta_g J_{hg}\right) + f_{LG} \tag{4}$$

where ρ_v (kg/m^3) is the water vapor mass concentration, θ_g (m^3/m^3) is gas phase volumetric content ($\theta_l + \theta_g = \phi$, being ϕ the soil porosity) and q_{gas} (m/s) is the gas phase flow. J_{hg} (kg/m^{2}s) is the hydrodynamic dispersion flow. This flow accounts for the diffusive and mechanical dispersive flows and it's expression is [*Bear and Bachmat*, 1991]:

$$J_{hg} = -\left(\frac{D_g}{\tau_g} + D_{vg}\right)\cdot\nabla\rho_v \tag{5}$$

where D_g (kg/m^2) is the molecular coefficient diffusion for the water vapor in air (depending on temperature [*Bird et al.*, 1960]). τ_g is the water vapor phase tortuosity and has been evaluated according the second model of Millington and Quirk, [*Millington*, 1959; *Millington and Quirk*, 1960], i.e. $\tau_g = \phi^{(2/3)}/\theta_g$. This model is appropriate in absence of experimental data [*Jin and Jury*, 1996]. Finally D_{vg} (kg/m^2) is the gas phase longitudinal dispersion coefficient and was estimated as $D_{vi} = \alpha_{Li}\cdot q_i/\theta_i$ (i=g,l) [*Bear*, 1972], where α_{Li} (m), longitudinal dispersivity in phase i, has been evaluated by various authors for different levels of soil saturation. Laboratory studies have shown that α_{Li} increases when the soil volumetric water content decreases. In this work we use a correlation made from simulation results [*Sahimi et al.*, 1986] and experimental data obtained by Haga et al.[*1999*]:

$$\alpha_{Li} = \alpha_{Li}\big|_{sat}\cdot\left[13.6 - 16\cdot\left(\theta_g/\phi\right) + 3.4\cdot\left(\theta_g/\phi\right)^5\right] \tag{6}$$

Additionally, the longitudinal dispersivity depends on the system size [*Gelhar et al.*, 1985]. In this work the longitudinal dispersivity values for saturated soil conditions, $\alpha_{Li\,Sat}$, has been chosen equal to 0.078 m as reported by *Biggar and Nielsen* [1976] for

saturated soil conditions in an agricultural field similar in size to our system.

The vapor water concentration in equilibrium with the liquid water located inside the porous, varies with the water vapor pressure ρ_{v_sat} (temperature dependent) and with liquid water pressure following the Kelvin's equation [*Bear and Bachmat*, 1991]

$$\rho_v = \rho_{v\_sat} \exp\left(\frac{P_l \cdot PM^a}{\rho_{liq} \cdot RT}\right) \tag{7}$$

where PM^a is the water molecular weight (kg/mol) and R is the universal gas constant (Pa m^3/K mol). The mass balance equation for the gaseous phase as a whole is [*Bear and Bachmat*, 1991]:

$$\frac{\partial \theta_g \rho_g}{\partial t} = -\nabla\left(\rho_g q_g\right) + f_{LG} \tag{8}$$

where the gas phase density ρ_g is the sum of the dry air and water vapor mass concentrations.

The mass balance (1), (4) and (8), together with the fluxes described in (2) and (5), the additional relations $k_r = k_r(\theta_l)$ and $\theta_l = \theta_l(P_l)$ and the description of the temperature dependence of the different properties, constitute a system that in order to be solved needs the temperature soil profiles as well as the boundary conditions for the top and bottom part of the system. In our case the boundary conditions for the bottom part have been set equal to $\partial P_l/\partial z = 0$, $\partial \rho_v/\partial z = 0$ and q_{gas}=0.

The evaporative flux at the surface is expressed as:

$$J_{evap} = -k'_{atm} \cdot \left(\rho_{atm} - \rho_v\big|_{z=0}\right) \tag{9}$$

where k'_{atm} is the atmospheric-side mass transfer coefficient between soil and atmosphere, which can be evaluated, for instance, by the semi-empirical correlation proposed by *Brutsaert* [1975] with modifications proposed by *Grifoll and Cohen* [1994]. In equation (9) ρ_{atm} is the vapor water mass concentration in the atmosphere phase.

2.2 Energy balance equation

It is commonly accepted that in soils the thermal transfer rate is much higher than the energetic fluxes associated with the mass fluxes. This assumption implies thermal equilibrium and will only break down at relatively high infiltration rates in coarse soils [*Milly*, 1982]. Under this assumption the energy balance in a representative control volume can be expressed as [*Bear and Bachmat*, 1991]:

$$\frac{\partial\left(\theta_l \rho_l u_l + \theta_g \rho_g u_g + (1-\phi)\rho_s u_s\right)}{\partial t} = \nabla\left(\rho_l q_l h_l + \rho_g q_g h_g + \theta_g J_{hg}\left(u_v - u_a\right) - \left(\lambda_{eff} + \theta_l D^H_{ml}\right)\nabla T\right) \tag{10}$$

where u_l, u_g y u_s (kJ/kg) are the specific internal energies corresponding to the liquid, gas and soil respectively, h_l y h_g (kJ/kg) are the specific enthalpies for the liquid and gas phase and $D^H_{ml} = \alpha_{lw} \cdot v_l \cdot \rho_l \cdot Cv_l$ is the mechanical dispersion coefficient corresponding to the sensible energy. Equation (10) includes enthalpic fluxes associated to the liquid and gas phase, energy differences associated with diffusive/dispersive fluxes, energy fluxes associated with the mechanical dispersion of the sensible energy as well as thermal conductivity. The effective thermal conductivity of soil, λ_{eff} (kJ/m K), has been

calculated using the equation proposed by Campbell [1994]

$$\lambda_{eff} = A + B\theta_l - (A - D)\exp\left(-(C\theta_l)^E\right) \quad (11)$$

where A, B, C, D and E are coefficients that depend on soil porosity, volume fraction of quartz and granulometric proportion of different minerals.

The top boundary condition for the energy balance equation takes into account incoming and outgoing radiative fluxes that arrive and depart from the soil surface, convective flux to the atmosphere as well as different soil heat fluxes due to different transport mechanisms. The dynamic variations of these fluxes, with daily cycle variations, depend on longitude and latitude as well as day of year [*Bras*, 1990]. The convective flux to the atmosphere depends on the wind speed and the soil roughness [*Brutsaert*, 1975; *Grifoll and Cohen*, 1994].

2.3 Numerical scheme solution

The one-dimensional transport equation for liquid water, vapor water, gas as a whole and energy, (equations 1, 4, 8 and 10 respectively) were solved by an implicit finite-difference approach. A one-dimensional version of the four coupled partial difference equations that compose the model was discretized using the control finite volume formulation [*Patankar*, 1980; *Grifoll and Cohen*, 1999]. The fluxes were discretized using a fully implicit scheme with a central differencing for the second derivatives and backward differencing for the first derivative [*Fletcher*, 1991]. In addition, a fully implicit time integration scheme was used.

The discretized energy and mass transport equations were solved using a triple

iterative scheme. For a given time step, a f_{LG} and temperature profile are assumed. Then the discretized model equation for liquid water movement is solved using the Newton-Raphson iteration procedure [*Press et al.*, 1989; *Grifoll and Cohen*, 1999].

The vapor water and gas as a whole transport equations, equations (4) and (8), are linear and therefore, once the discretized liquid water equations is solved, the q_{gas} and f_{LG} profiles can be easily obtained. This ultimate term is compared point by point against the supposed profile and in case that the discrepancy between points is higher than a 0.01%, the liquid water transport equation is solved again, using the latest f_{LG} profile obtained. Once the water transport solution is reached, the linear energy equation can be solved using the mass fluxes just obtained. The temperature profile obtained is then compared with the supposed profile used in the liquid water balance. If in any point the temperature difference between the two profiles is higher than 0.001 ºC the solution scheme restarts again.

For the range of simulations conducted in this work, the soil depth was set equal to 2 m and was divided into two zones. The first zone ($0 < z < 0.05$ m) has a constant step size equal to 0.001 m. In the second zone ($0.05\text{ m} < z < 2$ m) the step size increases progressively from 0.001 m to 0.1 m such that $\Delta z_i = r \cdot \Delta z_{i-1}$ with r equal to 1.1. A variable time step was selected between a minimum of 1s and a maximum of 3600 s to ensure enough numerical description of the temporal variations of the different dependent variables. The time step was automatically adjusted to ensure that in all cases the number of iterations needed for the liquid water transport solution was less or equal to 5. In all cases the local compliance of the classical restrictions when solving numerically linear transport equations (Courant and Péclet number limits) was monitored. Moreover, in all simulations was checked that further decreases of the grid

and time steps did not change appreciably the results.

The numerical algorithm for the solution of the liquid water was checked against the analytical solution given by Broadbridge an White [*1988*] for the case of constant rainfall for a Brindabella silt clay loam soil and results similar to those found by Grifoll and Cohen [*1996*] are obtained. The numerical algorithm for the energy transport was also checked against the analytical solution provided by Tyndall and Kunkel [*1999*] for the conductive heat transport equation with a sinusoidal temperature variation as a top boundary condition. A comparison between the numerical and analytical solution for the energy transport equation is given in figure 1.

3.- Results and discussion

Two different experimental works concerning water transport in the unsaturated zone under field conditions will be simulated [*Rose*, 1968 a,b; *Jackson*, 1973]. These works constitute a classical reference in the hydrological field and their simulation and comparison will verify the model ability to correctly describe the water and energy movement associated to a drying episode under natural field conditions. The results obtained will be used later to explore the importance of the different transport mechanisms as well as to explain the VMC daily variation observed in natural conditions

3.1 Rose experiment

The work of Rose [*1968* a,b] describes an experiment in which profiles of water

content and temperature were measured in the top 15 cm of bare soil for a period of 6 days and nights following saturation in natural field conditions. The experimental site was located at a frequently tilled plot in Alice Springs (Australia) (133º 50'E., 23º 45´S.). The work provides enough information about soil type characteristics, soil temperature variations as well as other meteorological data that have been used to reproduce with detail the soil scenario as well as the climatic conditions reported in Rose's experiment. Although no information concerning the period of the year when the experiment was done is available, the reported meteorological conditions seems to indicate that the experiment was conducted in July. Simulation results obtained considering different months (January and March) didn't display significant differences. The hydraulic functions used in the simulation correspond to Brooks and Corey [*1964*] and the hydraulic parameters have been adjusted from experimental measures given by Rose. This and other information about the soil properties are given in table 1 and 2. The model considers that both the air temperature and the atmospheric relative humidity describe a daily sinusoidal oscillation cycle with maximum and minimum values located at midday respectively. This and other pertinent meteorological parameter used in the simulation are given in table 3. The initial temperature and VMC soil profiles have been obtained from measured values reported by Rose.

Figure 2 exhibits the VMC evolution from saturation at three different depths (z= 0, 2.6 and 13.73 cm) along with experimental values obtained by Rose. For all but the lowest depth, both the simulated and measured VMC exhibit a sinusoidal fluctuation of daily period with a maximum value in the early hours of morning, around 04:00-06:00, and a minimum about 16:00. Figure 3 exhibits the temperature and vapor pressure soil profile corresponding to the night (04:00) and center of day (14:00) four days after the

beginning of the experiment. In the figure both the experimental and simulated results are depicted together. It is interesting to observe that the vapor pressure profile at 14:00 hr shows a maximum point around 1 cm depth. The extreme soil dryness near surface at 14:00 hr affects the vapor pressure profile through capillary effects expressed by equation 7. This inflection in the vapor pressure profile indicates the bottom boundary of the dry surface layer. Above the inflection point, in the dry layer, the water transport is mainly achieved in the vapor phase, while below this point, the transport is realized in liquid phase.

3.2 Jackson experiment

The second work that has been simulated correspond to the experimental study of Jackson [*1973*]. In this work Jackson studied the effects of diurnal water content variations in the evaporation process during a drying episode under natural field conditions. Similar to the experiment of Rose, soil water contents to 9 cm were measured in 1 cm increments at 0.5 hour intervals for 16 days during March after a 10 cm water irrigation process. The experimental site was located at Phoenix (Arizona). Important information about the soil type, climatic conditions as well as the period of the year is provided in Jackson's work. All this information has been used to describe with detail the simulation scenario. The hydraulic function employed for the θ_l (ψ) relation corresponds to Haverkamp et al. [*1977*] and a two parameter power law has been proposed to express the $k(\psi)$ relation. The hydraulic parameters have been obtained after adjusting the hydraulic functions to the experimental data provided by Jackson. Both the hydraulic functions and pertinent hydrological parameters are given

in table 1 and 2. Pertinent meteorological information is presented in table 3. The initial water moisture content profile has been obtained from experimental values corresponding to the first 8 cm for the 00:00 hr 7th of March, five days after the beginning of the experiment. In absence of experimental values for the initial temperature soil profile, the solution of the energy transport equation after a 24 hours simulation period has been used.

Figure 4 shows the measured volumetric water content for three days (from the 7th to the 9th of March five days after the starting of the experiment) in the 0-0.5 cm layer at 0.5 hour intervals. The measured values are presented along with the simulation results obtained for three different depths (z = 0, 2 and 5 mm). Both the experimental and simulated data exhibit a evolution similar to that found in Rose's experiment. The VMC variation observed is characterized by a sinusoidal daily oscillation with minimum values near midday and increases during the night hours. It is interesting to note the presence of elevated moisture content gradients near surface with moisture variations as high as 0.005 m^3/m^3 in a millimeter during the afternoon of the first day simulation.

3.3 Water transport mechanisms near surface

The good agreement observed between simulated and measured values presented so far, gives us some confidence about the model capacity to correctly describe the main mechanisms that govern the water and energy movement in the unsaturated soil near surface. Taking advantage of this feature, simulation results corresponding to Jackson's experiment will be used to explore the dynamic of the water fluxes that are responsible of the VMC variations observed in field conditions. In addition, a detailed accounting of

the different water fluxes located near surface will asses the importance and evolution of the transport mechanisms that contribute to the evaporative flux.

Figure 5 presents the evolution of the evaporation flux along with the water flux located at z = 1.5 mm. The evolution of the VMC for the first 1.5 mm in soil is also presented in the figure. The elapsed time presented correspond to the period that goes from the 7th to the 11th of March in Jackson's experiment. Both the evaporative and the water flux describe a daily sinusoidal variation with time decreasing amplitude and with maximum values that coincide with the moment of the day when the soil surface temperature reaches it's maximum value, approximately around midday. From the results presented we can observe that the slightly phase delay found between the cycle that governs the evaporative and water flux can explain the VMC evolution near surface. During the hottest daily hours, around midday, the VMC exhibits a strong decrease (↓). These hours coincide with the moment when the evaporative flux reaches its daily maximum value and surpass the water flux transported near surface. On the other hand, the daily hours when the VMC increases (↑), coincide with the night hours when the evaporative flux is lower than the water flux. Others authors have suggested different hypothesis to explain similar VMC variations observed. Rose for instance, [*1968* a,b] attributed to the coincidence in liquid and vapor flux directions by night and opposite by day, the pronounced increase in water content of the surface layers by night and decreased by day. Monji et al. [*1990*] attributed to the water movement due to temperature gradients in soils the observed moisture increase in soils. He concluded however that not reliable formulation were formulated. The explanation offered by Cahill and Parlange [*1998*] was that the increase in moisture content was caused in part by recondensation of water vapor from above. In our case, the accurate synchronization

observed between the VMC evolution and the different water fluxes, reinforces the hypothesis that the typical moisture content variations observed near soil surface in field conditions are governed by slightly differences between the evaporative and the water flux.

The liquid and vapor flux contribution to the total water flux located at z = 1.5 mm are given in figure 6 (a). The results presented make evident a progressively relieve between the liquid and vapor fluxes responsible of the water transport. During the first hours, when the moisture content in the top soil zone is high, the water transport is mainly achieved by the liquid flux. Later, and coinciding with the progressively soil drying process, the vapor flux becomes the main responsible of the upward water transport. These results make evident that the vapor flux is on the same order of magnitude as the liquid flux. The extremely low relative permeability values found during the daily hours when the VMC is close to the residual content, θ_{res}, reduces the liquid fluxes although the existence of important capillary pressure gradients near surface.

In order to determine the role of the various transport mechanisms involved in the water transport, figure 6 (b) presents the evolution of the different fluxes that contribute to the vapor flux located at z = 1.5 mm. Convective, diffusive and dispersive fluxes are presented along with the total vapor flux. The results obtained clearly show that both diffusive and dispersive fluxes are of comparable magnitude and contribute to the upward water transport. These results contrast with the minor contribution exhibited by the convective flux. Contrary to the theory proposed by Parlange et al. [*1998*] about the importance of the convective flux generated by thermal contraction and expansion of the soil air, our results indicate that the convective vapor contribution is small compared

with the diffusive of dispersive flux. Simulation results obtained for different cases, and not shown in the present work, indicate that although the volumetric air and water flows are similar, the five order magnitude difference between vapor and water liquid densities minimizes the convective vapor contribution to the water transport.

It is interesting to note the absence of downward thermally driven diffusion of water vapor in soils in the daytime. The presence of low VMC values near surface reduces, due to capillary effects, the relative humidity and the water vapor pressure profile allowing an upward flux even during the hottest daily hours. Similar to the results obtained by Yamanaka et al. [*1998*], simulation results obtained for the water vapor pressure profile exhibit a discontinuity near surface. The depth where this discontinuity appears indicates the location beneath the soil surface where evaporation takes place. The evaporative flux at each calculation node is expressed through the f_{LG} term present in equations 1, 4 and 8. This term considers the water transfer flux between the liquid and the gas phase and it is only noticeable in the extremely thin zone where evaporation occurs. This evaporation flux implies a small reduction of the water liquid volume and constitute an important water source for the gas phase. It also generates a convective flux in gas phase that contribute along with diffusive and dispersive fluxes to the water transport near surface.

The soil profile for the different water transport mechanisms as well as the total liquid and vapor fluxes are given in figure 7, (a) and (b), and correspond to the 14:00 and 02:00 hours after a 15 days simulation period. From the presented results, two distinct zones can be distinguished in the soil: an upper dry zone, $0 < z < 1$ cm, where water movement is due to vapor flux and a lower zone where liquid flux dominates the water transport. Results for the midday hours (14:00), figure 7 (a), demonstrates the important

role of the diffusive and dispersive transport mechanisms in the upper dry layer, with maximum contributions up to 77% and 33% respectively. Near the lower limit of the dry soil layer, the diffusive flux decreases and change from upward to downward. Coherent with the previously findings, the convective flux contribution is small. Results obtained for the 02:00 hours, figure 7 (b), make evident the decrease in the dispersive flux as well as the reduction of the evaporative flux during the night hours.

4.- Conclusions

A complete water and heat transport model for the unsaturated soil zone has been developed and implemented in a numerical code. The model has been favorably contrasted against experimental works obtained under field conditions.

The detailed accounting of all significant transport mechanisms and processes for the water and energy transport in porous media is shown to be enough to describe quantitatively the drying phenomenon without the help of any empirical parameter adjust. Simulation results obtained for a soil drying process have shown how the characteristic VMC daily variation observed near surface can be explained in terms of slightly differences between the evaporative and the water flux. Both the liquid and vapor flux contribute to the water transport near surface with comparable magnitude. The liquid flux is important and dominates the water movement during the initial hours, when the VMC is close to saturation, while the vapor flux increases its contribution as long as the soil dries. An upper dry and a lower wet zone are distinguished near surface. In the dry zone, the diffusive and dispersive transport mechanisms are of similar magnitude and are both responsible of the vapor flux. In the wet lower zone, the

convective liquid flux is the main transport mechanism while the diffusive flux decreases and changes from upward to downward direction. It is important to note that both the diffusive and dispersive fluxes have been evaluated using semi-empirical parameters, like the tortuosity and the longitudinal dispersivity, obtained from equations based on field and laboratory experiments.

5.- References

Bear, J. and Y. Bachmat, Introduction to modeling of transport phenomena in porous media, Theory and applications of transport in porous media, Ed. (Jacob Bear), Volum 4, Kluwer Academic Publishers, Dordrecht / Boston / Londres, 1991.

Bear, J., *Dynamics of fluids in porous media*, Dover, New York, 1972.

Biggar, J.W: i D.R: Nielsen, Spatial variability of the leaching characteristics of a field soil, *Water Resour. Res.*, 1, 78-84, 1976.

Boulet, G., I. Braud and M. Vauclin, Study of the mechanisms of evaporation under arid conditions using a detailed model of the soil-atmosphere continuum. Application to the EFEDA and experiment, *Journal of Hidrology*, 193, 114-141, 1997.

Bras R.L., *Hydrology an introduction to hydrologic science*, Addison-Wesley, 1990.

Broadbrige P. and I. White, Constant rate infiltration. A versatile nonlinear model, 1. Analytic solution. *Water Resour. Res*., 4, 543-550, 1988.

Brooks, R.H. and A.T. Corey, Hydraulic properties of porous media, *Hydrol. Pap. 3*, Colorado State University, Ft. Collins, 1964.

Brutsaert W., A theory for local evaporation (or heat transfer) from rough and smooth surfaces at ground level, *Water Resour. Res.*, 4, 543-550, 1975.

Cahill A.T. and M.B. Parlange, On water vapor transport in field soils, *Water Resour. Res.*, 34(4), 731-739,1998.

Cahill A.T. and M.B. Parlange, Reply, *Water Resour. Res.*, 36(10), 3107-3110, 2000.

Campbell G.S., Soil physics with BASIC-Transport models for soil-plant systems, Develeopment in Soils 14, Elsevier Science B.V., Amsterdam, 1994.

Cary, J.W., Soil moisture transport due to thermal gradients: Practical aspects, *Soil Sci. Soc. Am. Proc.*, 30(4), 428-433, 1966.

Fletcher, C.A.J., *Computational techniques for fluid dynamics, 1*. Springler Verlag, BErlin, 1991.

Grant S.A. and A. Salehzadeh, Calculation of temperature effects on wetting coefficients of porous solids and their capillary pressure functions, *Water Resour. Res.*, 32, 261-270, 1996.

Grifoll J. and Y. Cohen, A front-tracking numerical algorithm for liquid infiltration into nearly dry soils, *Water Resour. Res.*, 35, 2579-2585, 1999.

Grifoll J. and Y. Cohen, Contaminant migration in the unsatured soil zone: the effect of rainfall and evapotranspiration, *Journal of contaminant hydrology*, 23, 186-211, 1996.

Grifoll J. and Y. Cohen, Chemical volatilization from the soil matrix: Transport through the air and water phases, *J. Hazard. Mater.*, 37, 445-457, 1994.

Haga, D., Y. Niibori and T. Chida, Hydrodynamic dispersion and mass transfer in unsatured flow, *Water Resour. Res.*, 35, 1065-1077, 1999.

Hanks R.J., Gardner H.R. and Fairbourn, M.L., Evaporation of water from soils as influenced by drying with wind or radiation, Proc. Soil Sci. Soc. Am., 31(5),583-593, 1967.

Haverkamp, R., M. Vauclin, J. Touma, P.J. Wierenga and G. Vachaud, A comparison of numerical simulation models for one-dimensional infiltration, *Soil Science Society of America Journal*, 41, 286-294, 1977.

Jackson, R.D., Diurnal Changes in soil water content during drying, A R.R. Bruce et al. (Editors) Field soil water regime. Special Pub. 5., *Soil Sci. Soc. Amer. Proc.*, 37-55, 1973.

Jackson, R.D., R.J. Reginato, B.A. Kimball and F.S. Nakayama, Diurnal soil-water. evaporation: comparison of measured and calculated soil-water fluxes, *Soil Sci. Soc. Amer. Proc.*, 38, 861-866, 1974.

Jin Y. and A. Jury, Characterizing the dependence of gas diffusion coefficient on soil properties, *Soil Sci. Soc. Am. J.*, 60, 66-71, 1996.

Millington R.J. and J.P. Quirk, Transport in porous media, A F.A. van Beren et al. (Editors), *Trans. Int. Congr. Soil Sci. 7th*, 1, 97-107, Madison, WI. 14-24, Elsevier, Amsterdam, 1960.

Millington R.J., Gas diffusion in porous media, *Science*, 130, 100-102, 1959.

Milly, P.C.D., Moisture and heat transport in hysteretic, inhomogeneous porous media: A matric head-based formulation and a numerical model, *Water Resour. Res.*, 18(3), 489-498, 1982.

Milly, P.C.D., A simulation analysis of thermal effets on evaporation from soil, *Water Resour. Res.*, 20(8), 1087-1098, 1984.

Milly, P.C.D., Effects of thermal vapor diffusion on seasonal dynamics of water in the unsaturated zone, *Water Resour. Res.*, 32(3), 509-518, 1996.

Monji N., Hamotami K. and Y. Omoto, Dynamic behavior of the moisture near the soil-atmosphere boundary, *Bull. Univ. Osaka Pref.*, Ser, B, 42, 61-69, 1990.

Parlange M.B., A.T. Cahill, D.R. Nielsen, J.W. Hopmans and O. Wendroth, Review of heat and water movement in filed soils, *Soil&Tillage Research*, 47, 5-10, 1998.

Patankar S.V., Numerical heat transfer and fluid flow, McGraw-Hill, New York, 1980.

Philip J.R: and D.A. de Vries, Moisture movement in porous media under temperature gradients, *Transactions American Geophysical Union*, 38(2), 222-231,1957.

Press W.H, B.P. Flannery, S.A. Teukolsky and W.T. Vetterling, Numerical Recipes, Cambridge University Press, Cambridge.

Rose C.W., Water transport in soil with a daily temperature wave. I Theory and experiment,., *Aust. J. Soil. Res.*, 6, 31-44, 1968 (a).

Rose C.W., Water transport in soil with a daily temperature wave. II Analysis, *Aust. J. Soil. Res.*, 6, 31-44, 1968 (b).

Sahimi, M., A. Heiba, H. Davis and L. Scriven, Dispersion in flow through porous media, II. Two phase flow. *Chem. Eng. Sci.* 41, 2123, 1986.

Saravanapavan, T. and G.D. Salvucci, Analysis of rate-limiting processes in soil evaporation with implications for soil resistance models, *Advances in water resources*, 23, 493-502, 2000.

Scanlon B.R. and P.C.D. Milly, Water and heat fluxes in desert soils 2. Numerical simulations, *Water Resour. Res.*, 30(3), 721-733, 1994.

Tyndall J.A. and J.R. Kunkel, Unsatured zone hydrology for scientists and engineers, Prentice Hall. New Jersey, 1999.

Van Genuchten M.Th. and P.J.Wierenga, Mass transfer studies in sorbing porous media, II. Experimental evaluation with tritium (3H2O)1, *Soil Sci. Soc. Am. J.*, 41, 272-278, 1977.

Van Genuchten M.Th., P.J. Wierenga and G.A. O'Connor, Mass transfer studies in sorbing porous media, III. Experimental evaluation with 2,4,5T, *Soil Sci. Soc. Am. J.*, 41, 278-285, 1977.

Wescot D.W. and P.J. Wierenga, Transfer of heat by conduction and vapor movement in a closed soil system. *Soil Sci. Soc. Am. Proc.*, 38, 9-14, 1974.

Yamanaka, T., A. Takeda and J. Shimada, Evaporation beneath the soil surface: some observational evidence and numerical experiments, *Hydrol. Process*., 12, 1998.

TABLES

Table 1. Hydrological parameters.

	Rose experiment Soil	Jackson experiment soil
θ_{sat} (m^3/m^3)	0.4	0.388
θ_{res} (m^3/m^3)	0.015	$5 \cdot 10^{-3}$
K_s (m/s)	$1.58 \cdot 10^{-5}$	$1.98 \cdot 10^{-6}$
ψ_b (m)	0.0586	
λ	0.3	
α		3.953
β		0.398
a		$6.664 \cdot 10^{-3}$
b		-2.09

[a] Calculated value with T=298K and RH=50%

Table 2. Hydraulic functions

	$\theta_l(\psi)$	$k_r(\psi)$
Rose simulation [a]	$\theta_l = \left(\frac{\psi_b}{\psi}\right)^{\lambda} \cdot (\varepsilon - \theta_{wr}) + \theta_{wr}$; $\psi < \psi_b$ $\theta_l = \varepsilon$; $\psi > \psi_b$	$k_r = \left(\frac{\psi_b}{\psi}\right)^{\eta}$; $\psi < \psi_b$ $k_r = 1$; $\psi > \psi_b$
Jackson simulation	$\theta_l = \frac{\alpha(\theta_s - \theta_r)}{\alpha + \lvert\psi\rvert^{\beta}} + \theta_r$ [b]	$k_r = a \lvert\psi\rvert^{b}$ [c]

[a] Where ψ is the matric potential. ψ can be related with P_l through, $\psi = {}^{P_l}\!/_{\rho \cdot g}$. ψ_b is the the bubbling pressure and η=2+3·λ, [*Brooks and Corey*, 1964].

[b] [Haverkamp et al., 1977].

[c] Proposed relationship.

Table 3. Simulation parameters

	Rose Experiment	Jackson Expariment
Longitude	133º5′ E	112º1′ W
Latitude	23º45′ S	33º8′ N
Date (dd/mm)	01/01	01/03
Hour (hh:mm)	17:00	00:00
Hr_a ***(%)*** [a]	50	70
T_a ***(ºC)*** [b]	13.5	12.5
A_{Hr}***(%)***[c]/A_T ***(ºC)*** [c]	-10/6.5	-10/7.5
ϕ ***(º)***[d]	-105	-105
z_0 ***(m)*** [e]	0.01	0.01
z_r ***(m)*** [f]	2	2
u (m/s) [g]	5	2.95

[a] Relative humidity at midday
[b] Atmospheric temperature at midday
[c] Daily oscillation amplitude for the relative humidity and temperature
[d] Time phase
[e] Soil rugosity
[f] Reference height
[g] Wind speed

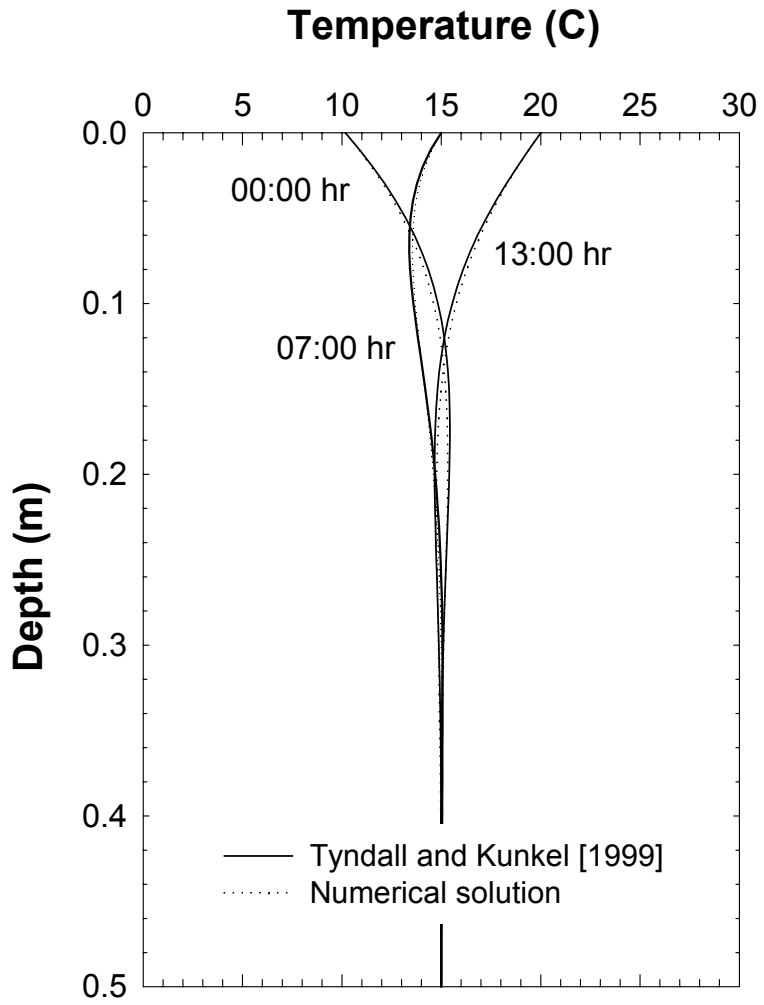
Temperature (C)
0
5
10
15
20
25
30
0.0
0.1
0.2
0.3
0.4
0.5
Depth (m)
00:00 hr
07:00 hr
13:00 hr
Tyndall and Kunkel [1999]
Numerical solution

Figure 1

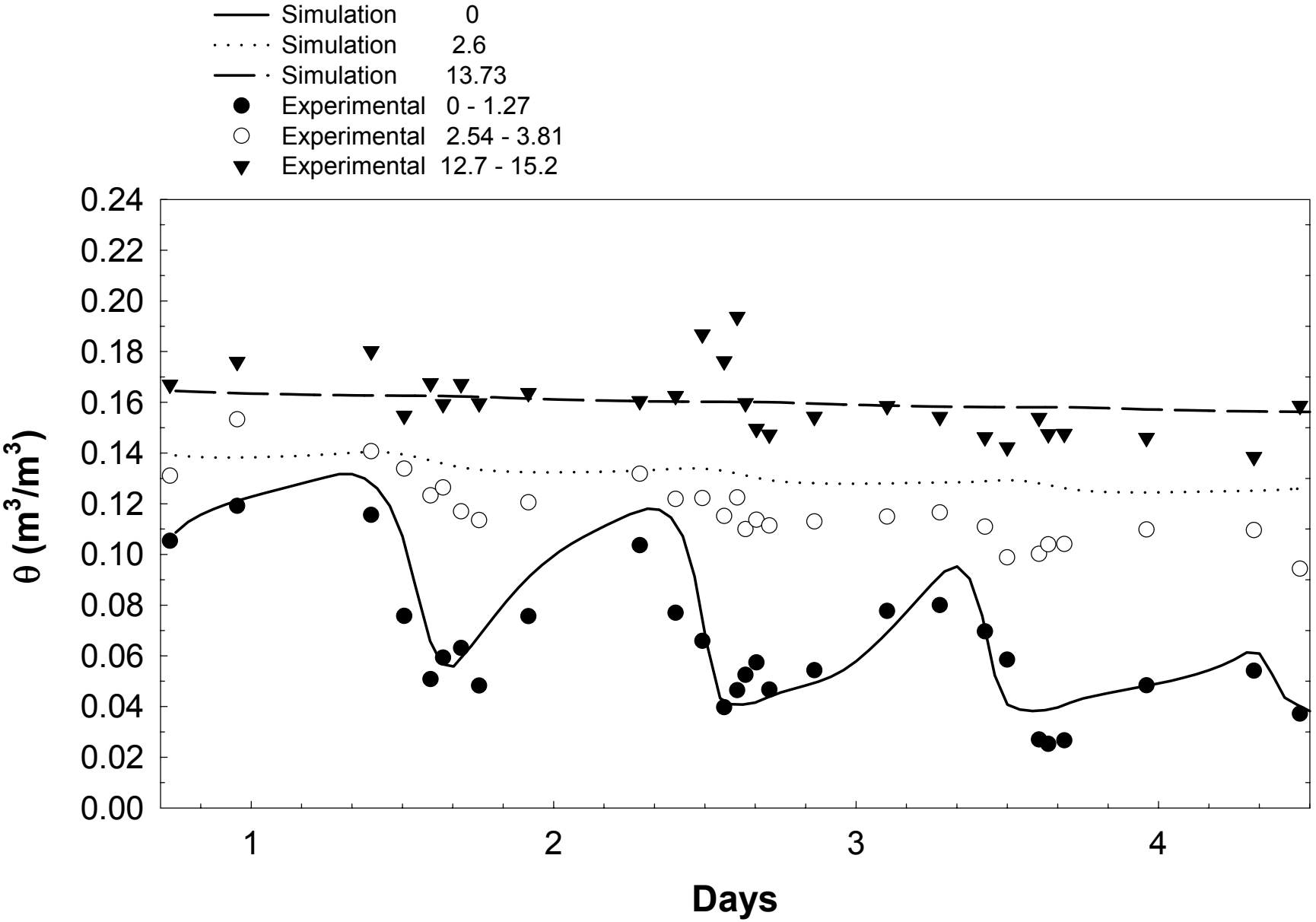
Simulation 0
Simulation 2.6
Simulation 13.73
Experimental 0 - 1.27
Experimental 2.54 - 3.81
Experimental 12.7 - 15.2
θ (m³/m³)
0.24
0.22
0.20
0.18
0.16
0.14
0.12
0.10
0.08
0.06
0.04
0.02
0.00
1
2
3
4
Days

Figure 2

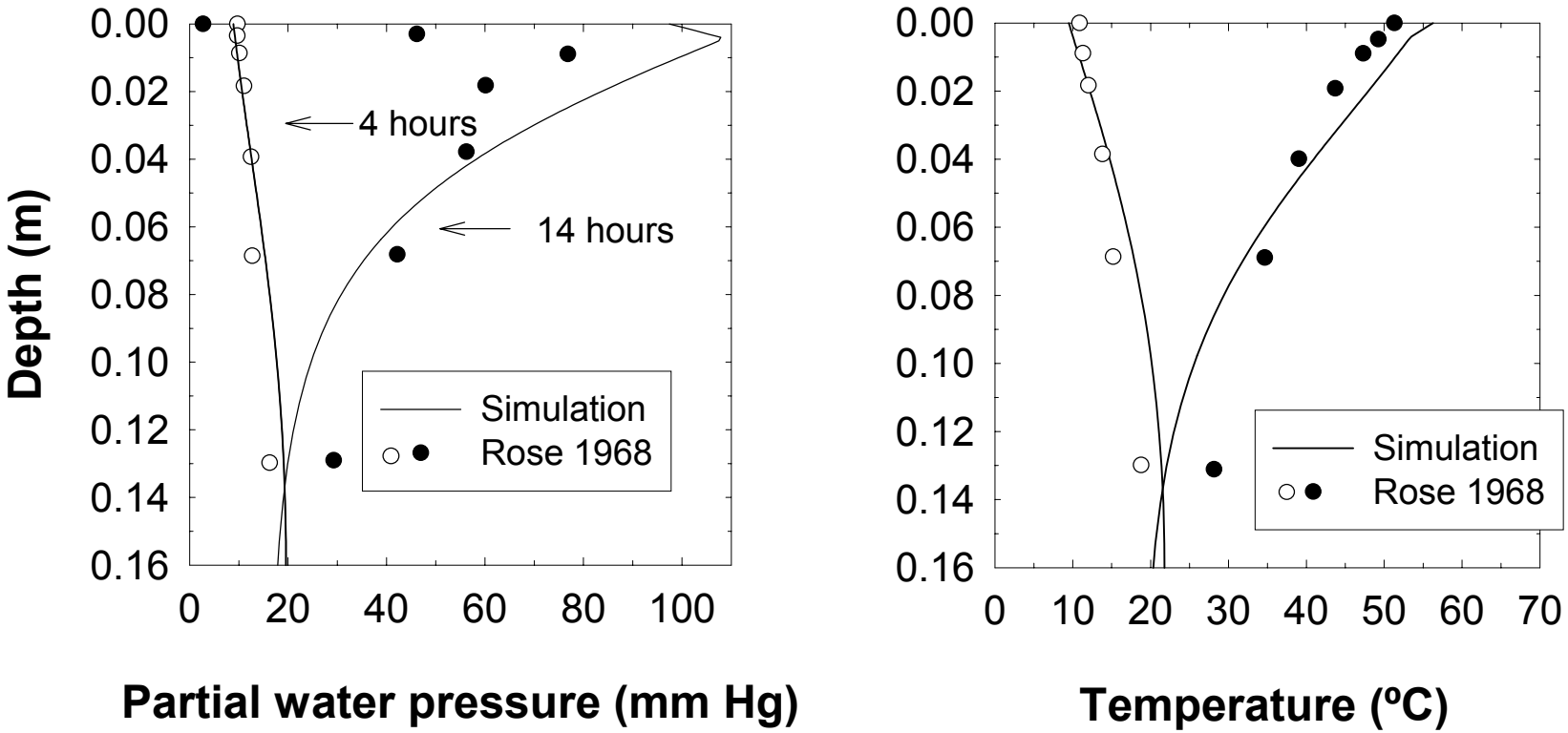
Depth (m)
0.00
0.02
0.04
0.06
0.08
0.10
0.12
0.14
0.16
4 hours
14 hours
Simulation
Rose 1968
0
20
40
60
80
100
Partial water pressure (mm Hg)
0
10
20
30
40
50
60
70
Temperature (ºC)

Figure 3

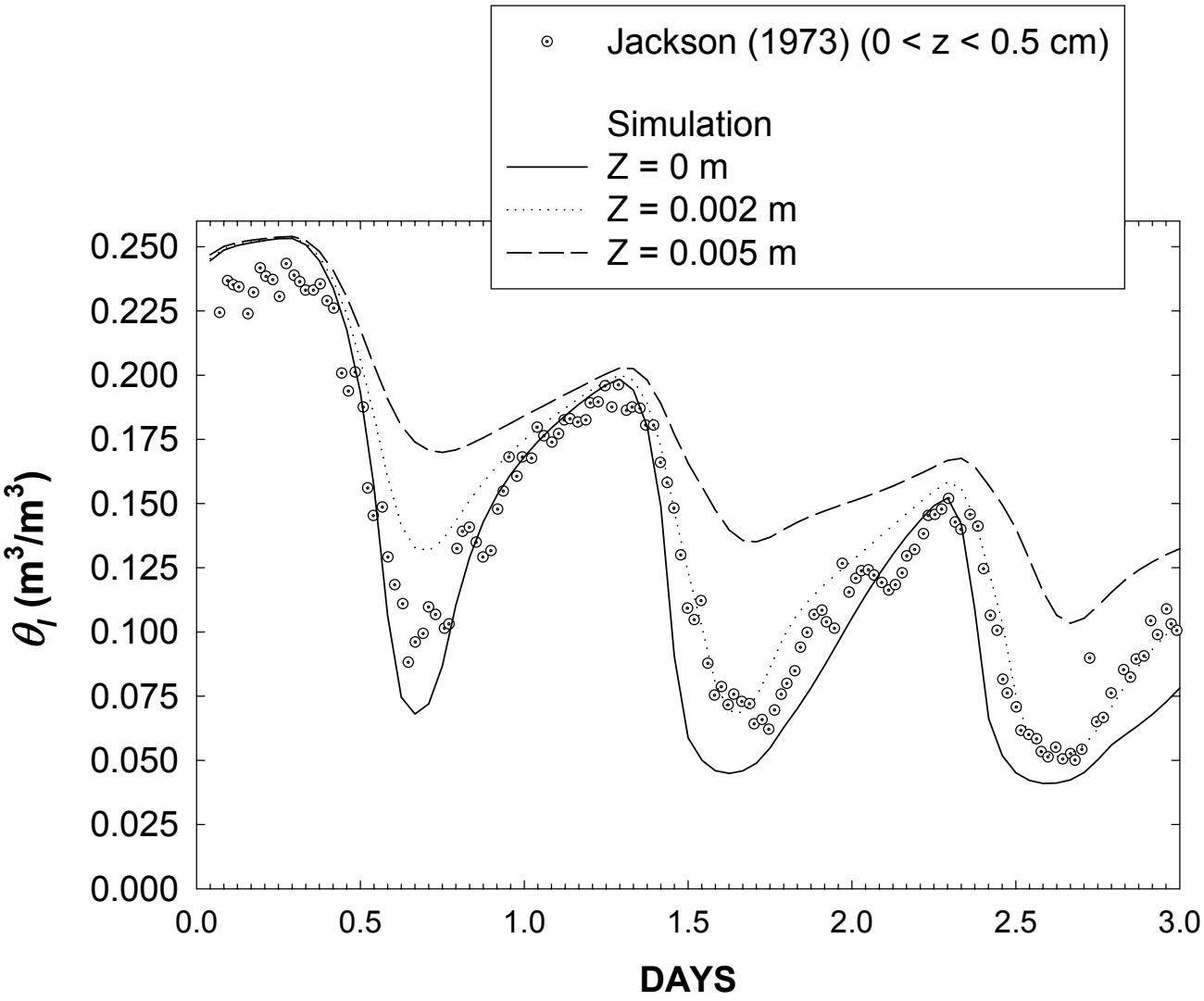
Jackson (1973) (0 < z < 0.5 cm)
Simulation
Z = 0 m
Z = 0.002 m
Z = 0.005 m
0.250
0.225
0.200
0.175
0.150
0.125
0.100
0.075
0.050
0.025
0.000
θl (m3/m3)
0.0
0.5
1.0
1.5
2.0
2.5
3.0
DAYS

Figure 4

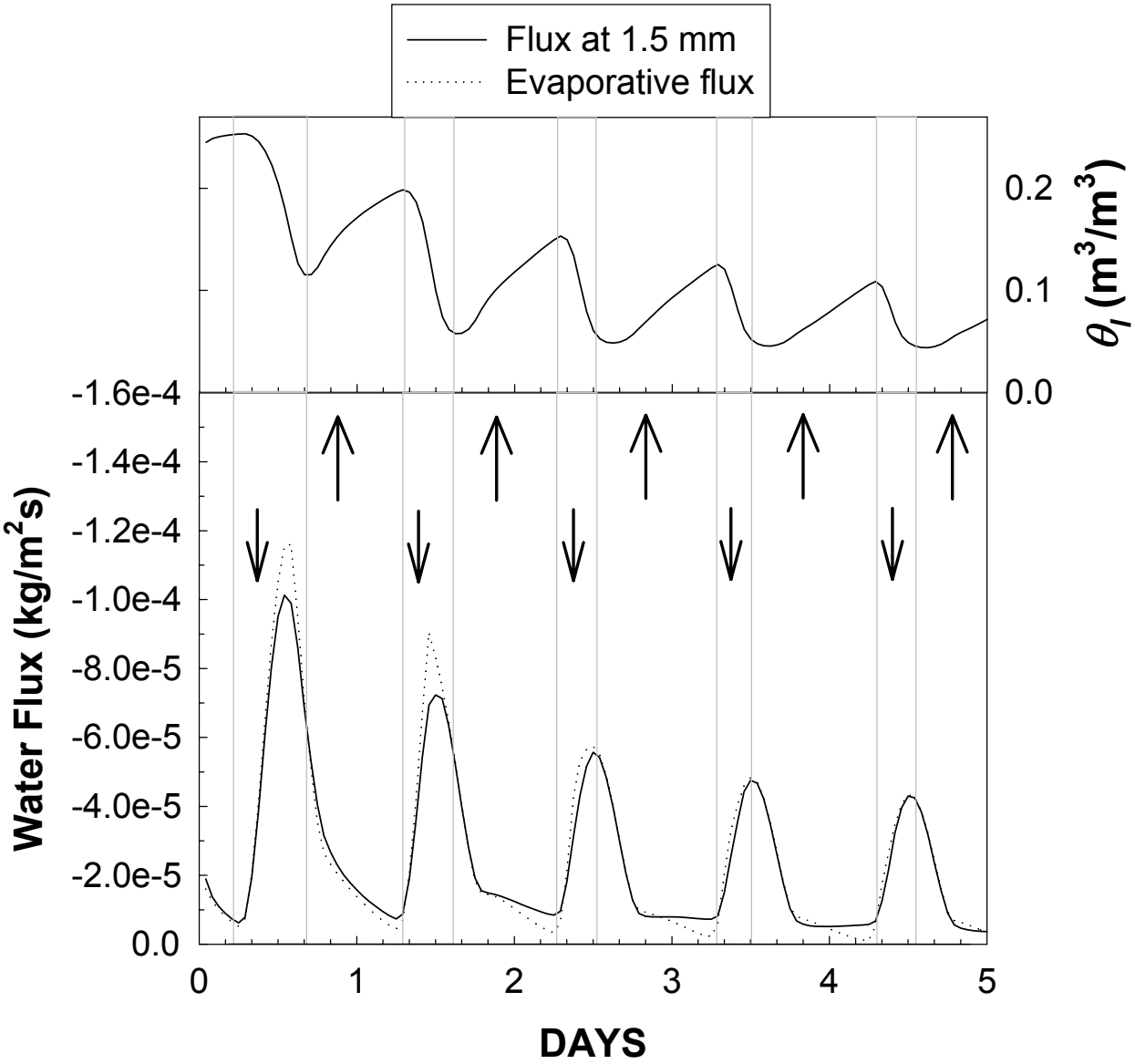
Flux at 1.5 mm
Evaporative flux
0.2
0.1
0.0
θ_l (m^3/m^3)
-1.6e-4
-1.4e-4
-1.2e-4
-1.0e-4
-8.0e-5
-6.0e-5
-4.0e-5
-2.0e-5
0.0
Water Flux (kg/m^{2}s)
0
1
2
3
4
5
DAYS

Figure 5

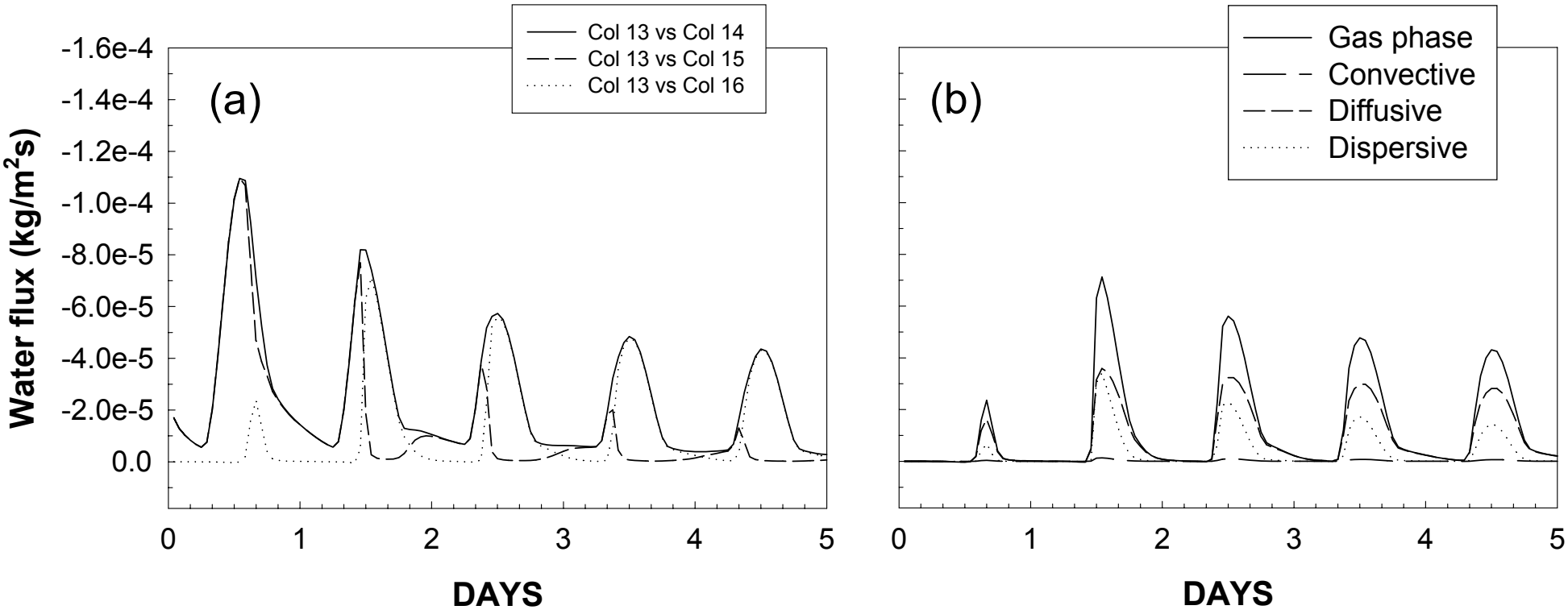
Water flux (kg/m²s)
-1.6e-4
-1.4e-4
-1.2e-4
-1.0e-4
-8.0e-5
-6.0e-5
-4.0e-5
-2.0e-5
0.0
(a)
Col 13 vs Col 14
Col 13 vs Col 15
Col 13 vs Col 16
0
1
2
3
4
5
DAYS
(b)
Gas phase
Convective
Diffusive
Dispersive
0
1
2
3
4
5
DAYS

Figure 6

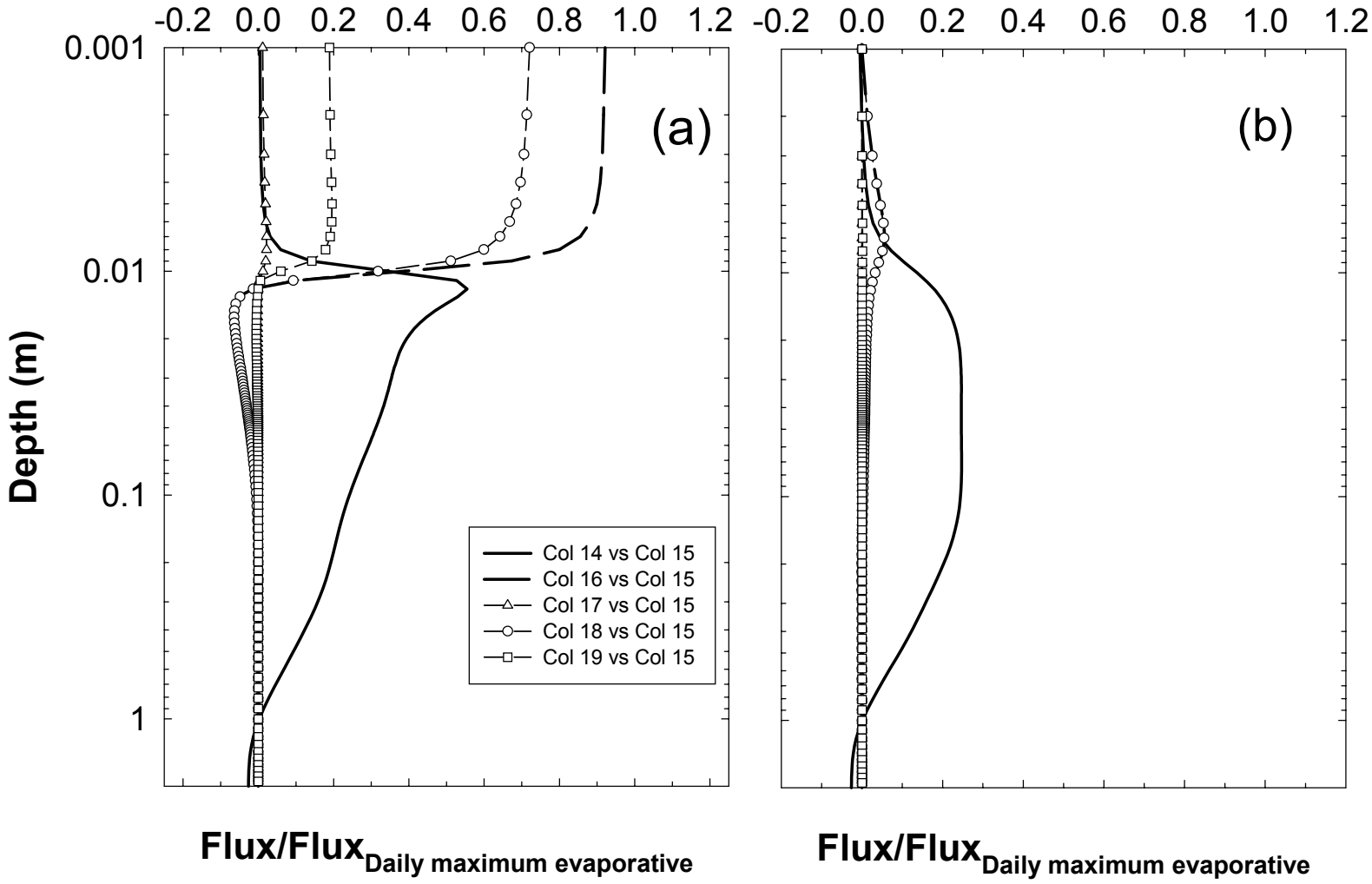
-0.2 0.0 0.2 0.4 0.6 0.8 1.0 1.2
0.001
0.01
0.1
1
Depth (m)
(a)
(b)
Col 14 vs Col 15
Col 16 vs Col 15
Col 17 vs Col 15
Col 18 vs Col 15
Col 19 vs Col 15
Flux/Flux Daily maximum evaporative
Flux/Flux Daily maximum evaporative

Figure 7